



OPEN

Formation of quantum dots in GaN/AlGaIn FETs

Tomohiro Otsuka^{1,2,3,4,✉}, Takaya Abe¹, Takahito Kitada¹, Norikazu Ito⁵, Taketoshi Tanaka⁵ & Ken Nakahara⁵

GaN and the heterostructures are attractive in condensed matter science and applications for electronic devices. We measure the electron transport in GaN/AlGaIn field-effect transistors (FETs) at cryogenic temperature. We observe formation of quantum dots in the conduction channel near the depletion of the 2-dimensional electron gas (2DEG). Multiple quantum dots are formed in the disordered potential induced by impurities in the FET conduction channel. We also measure the gate insulator dependence of the transport properties. These results can be utilized for the development of quantum dot devices utilizing GaN/AlGaIn heterostructures and evaluation of the impurities in GaN/AlGaIn FET channels.

GaN and the heterostructures are attractive materials because of their interesting electronic properties: the large direct bandgap, the high electron densities and mobilities. They are utilized in light-emitting diodes^{1–3}, power and high-frequency electronics devices^{4–6}. In electronic device applications, GaN/AlGaIn heterostructures are important structures. High density and high mobility 2DEG is formed at the interface^{7,8}. The 2DEG is also investigated on the viewpoint of spin-orbit interactions^{9–11} and electron spin resonances¹². Quantum nanostructures can be fabricated from the heterostructure by utilizing nano-fabrications. Quantum point contacts¹³ and single electron transistors¹⁴ are reported. GaN/AlGaIn nanowires^{15,16} and self-assembled GaN islands¹⁷ are also used to form quantum dots. Then GaN and the heterostructures are attractive also in quantum devices utilizing the electronic properties.

Quantum dots can be formed also by intrinsic impurity potentials not only by the electric gates or edges defined structures. In Si FETs, the formation of quantum dots by electrical potentials induced by dopants is reported^{18–20}. Dopants themselves work as quantum dots and control of the dopants²¹ is used for quantum bit applications^{22–26}, which is studied for quantum information processing^{27,28}. The stronger confinement by the dopant makes larger quantization energies and this enables high-temperature operation of the semiconductor quantum bits²⁹.

In this paper, we measure electron transport through GaN/AlGaIn FETs at cryogenic temperature. We observe non-monotonic modulation of the current indicating formation of quantum dots near the pinch-off condition of the FET channel. Multiple quantum dots are formed in the potential fluctuations induced by the impurities near the conduction channel. We also measure the gate insulator dependence.

Results

Device and FET properties. Figure 1a shows a schematic of the layer structure of the device. GaN and AlGaIn layer is grown on the Si substrate by chemical vapor deposition. At the interface between the GaN and AlGaIn layers, 2DEG is formed. The typical values of the electron density and the mobility are $6.7 \times 10^{12} \text{ cm}^{-2}$ and $1700 \text{ cm}^2 \text{ V}^{-1} \text{ s}^{-1}$. Source and drain contacts are prepared by Ti/Al. A TiN gate electrode is deposited on the insulator of SiN and SiO₂. SiN is grown in-situ just after the growth of the GaN/AlGaIn. An optical image of the device is Fig. 1b. The gate electrode is placed between the source and the drain contacts. The gate length and the gate width are 1.4 μm and 150 μm , respectively.

¹Research Institute of Electrical Communication, Tohoku University, 2-1-1 Katahira, Aoba-ku, Sendai 980-8577, Japan. ²Center for Spintronics Research Network, Tohoku University, 2-1-1 Katahira, Aoba-ku, Sendai 980-8577, Japan. ³Center for Science and Innovation in Spintronics, Tohoku University, 2-1-1 Katahira, Aoba-ku, Sendai 980-8577, Japan. ⁴Center for Emergent Matter Science, RIKEN, 2-1 Hirosawa, Wako, Saitama 351-0198, Japan. ⁵ROHM Co., Ltd, 21 Saiinnmizosakicho, Ukyo-ku, Kyoto 615-8585, Japan. ✉email: tomohiro.otsuka@riec.tohoku.ac.jp

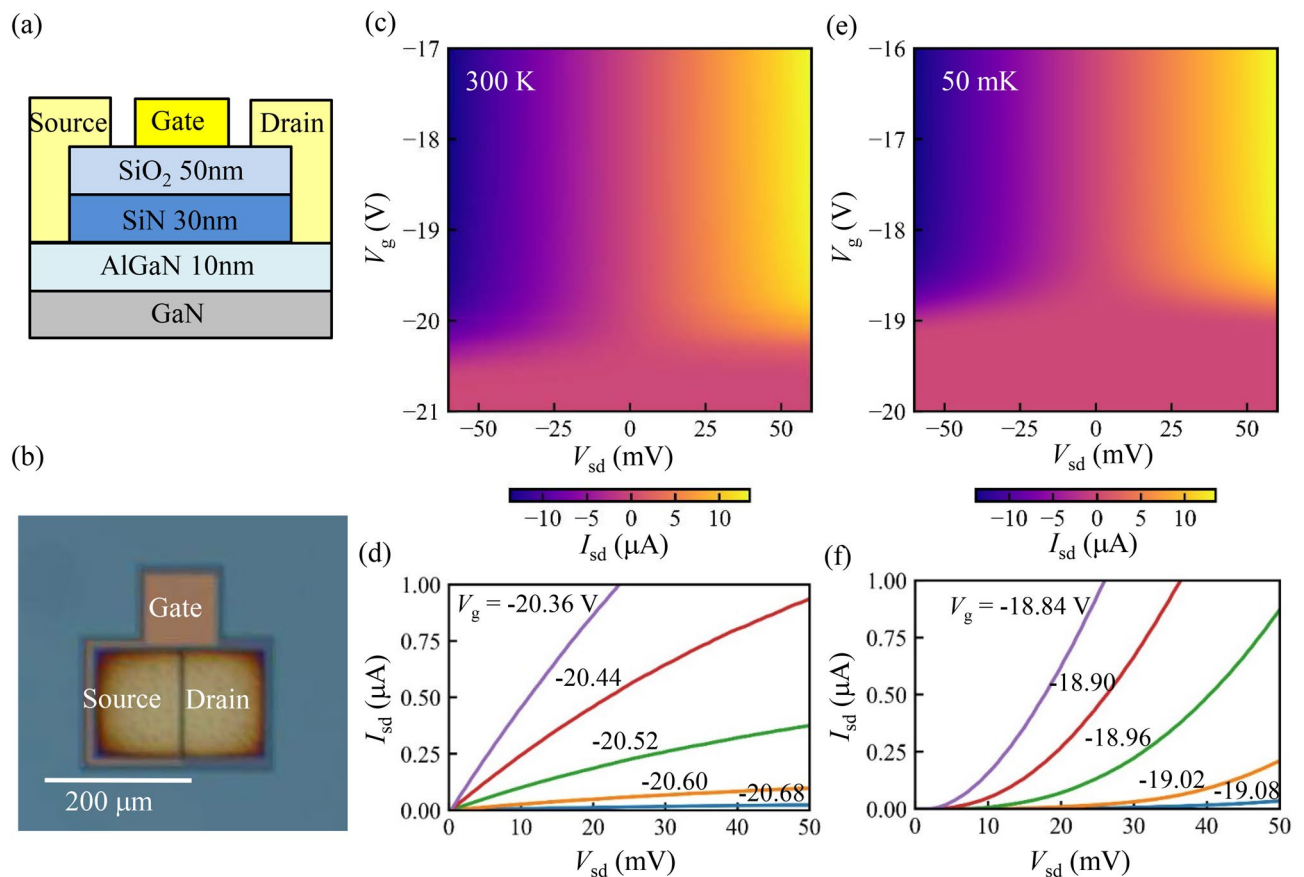


Figure 1. (a) Schematic of the layer structure of the device. 2 DEG is formed at the interface between GaN and AlGaIn. (b) Optical image of the device. The gate electrode with 1.4 μm gate length is placed between the source and the drain. (c–f) Current through the GaN/AlGaIn FET as a function of the source-drain bias voltage V_{sd} and the gate voltage V_g at 300 K (c,d) and 50 mK (e,f).

The current between the source and the drain contacts I_{sd} is measured as a function of the applied source-drain bias voltage V_{sd} and the gate voltage V_g . We measure the current through the device at the room temperature 300 K and cryogenic temperature 50 mK. The device is cooled down by a dilution refrigerator.

Figure 1c and d show the measured current through the GaN/AlGaIn FET I_{sd} at the room temperature 300 K. In $V_g > -20.7$ V, the FET channel is opened and the current flows depending on V_{sd} . In the measurement, two 1 kΩ resistors, which is used for low pass filters designed for the cryogenic measurement, are inserted in series to the device and this limits the current in the open condition of the FET. Around $V_g \sim -20.7$ V, the conduction channel is depleted. No current flows in more negatively gated region $V_g < -20.7$ V.

Figure 1e and f show the measured I_{sd} at the cryogenic temperature 50 mK. The conduction channel remains at this temperature in $V_g > -19.1$ V. The depletion of the conduction channel occurs around $V_g \sim -19.1$ V. The pinch-off voltage shifts 1.6 V positively compared to the result at the room temperature. This is induced by the suppression of the thermally induced carriers at the cryogenic temperature. More detail of the sheet resistance and the contact resistance will be revealed by transmission line measurement.

Formation of quantum dots. Figure 2a shows the current through the FET near the depletion condition of the 2DEG. The current is suppressed around the zero bias and non-linear I–V properties are observed in this region. A numerical derivative of the measured current as a function of the source-drain bias voltage dI_{sd}/dV_{sd} is shown in Fig. 2b. The current I_{sd} is blocked around the zero bias condition $V_{sd} \sim 0$. The width of the blocked region is modulated by the gate voltage V_g and Coulomb diamonds are observed. The size of the diamonds becomes larger in more negative values of V_g and this reflects that the dot size becomes smaller and the charging energy becomes larger. Note that the faint vertical lines around the outside of the diamonds are the measurement artifact that originates from the output voltages of the source measure unit used in this measurement.

Figure 3a shows the closed up image of the Coulomb diamonds. In this small current condition, we use a current preamplifier to measure the current instead of the source measure unit and the measurement artifact like in Fig. 2b is not there. In the Coulomb blocked region, the conductance is smaller than 0.1 nS. The current enhancement by the excited states is also observed as lines outside of the Coulomb diamonds. Quantum dots are formed in the conduction channel of the FET.

The visible lines mostly have the same slope and this indicates that the dot is asymmetrically coupled to the leads: the dot is strongly coupled to one of the leads. The voltage drop by forming the large in-series resistance

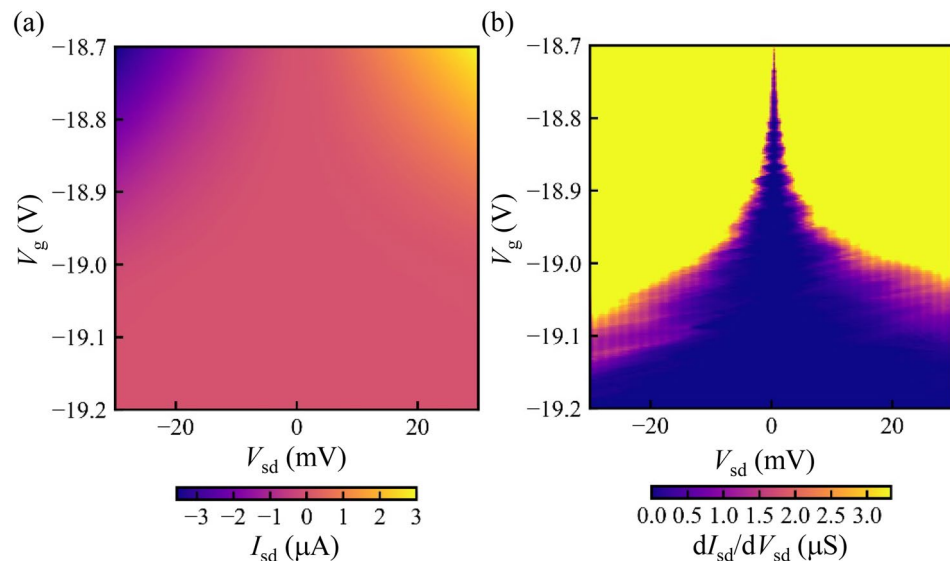


Figure 2. (a) Current through the FET as a function of the source-drain bias voltage V_{sd} and the gate voltage V_g at 50 mK near the depletion condition of the 2DEG. (b) The numerical derivative of the measured current as a function of the source-drain bias voltage dI_{sd}/dV_{sd} . Non-monotonic modulation of the current and Coulomb diamond structures are observed.

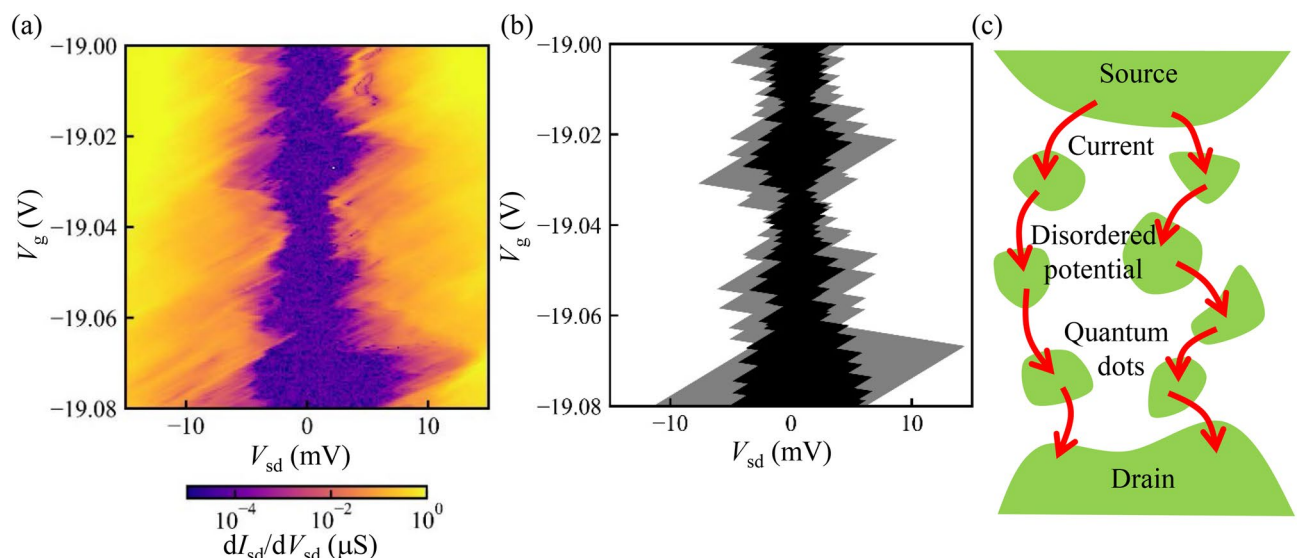


Figure 3. (a) Numerical derivative of the current as a function of the source-drain bias voltage. Coulomb diamonds are observed. (b,c) Schematic of the one possible configuration of the quantum dots (c) and the expected Coulomb diamonds (b). Electrostatic potential will be disordered by the impurities and defects and the quantum dots are formed at the potential minima. Here we assumed that three and four quantum dots are coupled in series, and these are coupled in parallel. The overlapped Coulomb diamonds show gaps around the zero bias conditions.

in the conduction channel is negligible, which can be evaluated by inverting the source and the drain contacts in the measurement³⁰. The diamonds are not completely closed at $V_{sd} = 0$ in Fig. 3a. This shows that multiple quantum dots are formed in this device.

Discussion

There are no small fine gates or structures to define quantum dots intentionally in this device. The quantum dots will be formed by the disordered potential induced by the impurities or defects near the conduction channel. Near the depletion of the 2DEG, electrons are trapped in the potential minima of the disordered potential. The confinement induces the single-electron charging effect and the size quantization effect. The former produces the Coulomb diamonds. The latter modifies the size of the diamonds and produces the excited state lines.

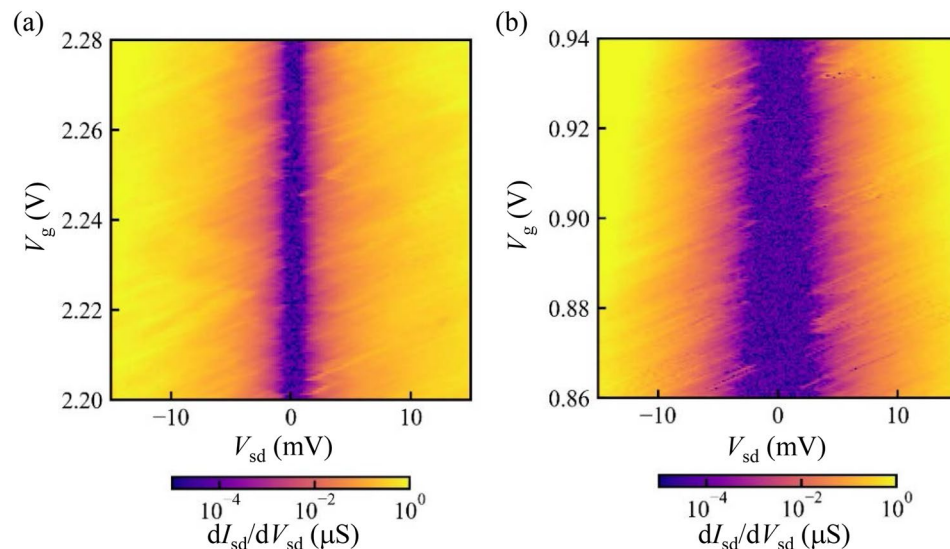


Figure 4. (a,b) Numerical derivative of the current as a function of the source-drain bias voltage observed in other samples with different insulators SiO₂ (a) and SiN/SiO₂.

Figure 3c is a schematic of one possible configuration of the formed quantum dots. Three and four quantum dots are coupled in series, and these are coupled in parallel. The resulting Coulomb diamonds become the overlap of the diamonds of each dot in the case of series connection in a simple approximation³¹. Figure 3b shows the result when we assume the three quantum dots with charging energies $E_{C1}, E_{C2}, E_{C3} = 2.6, 2.3, 3.0$ meV, orbital level spacing $\Delta\epsilon_1, \Delta\epsilon_2, \Delta\epsilon_3 = 0.97-11, 0.81-4.1, 0.65-2.9$ meV and the four quantum dots with charging energies $E_{C4}, E_{C5}, E_{C6}, E_{C7} = 1.4, 1.2, 1.1, 1.3$ meV, orbital level spacing $\Delta\epsilon_4, \Delta\epsilon_5, \Delta\epsilon_6, \Delta\epsilon_7 = 0.24-3.7, 0.18-4.2, 0.18-4.8, 0.24-4.6$ meV. The gray area indicates the partially blocked region by the three dots and the black area indicates the fully blocked region by the three and four dots. The model capture the main feature of Fig. 3a.

To study the growth condition dependence of the quantum dot formation, we measure other samples with different gate insulators and fabrication processes, which induce different disorder densities. In these new samples, the insulator is fabricated after taking out the samples from the growth chamber of GaN/AlGaIn and etching processes. The gate length is $0.6 \mu\text{m}$. Higher disorder densities are expected compared to the previous sample which has SiN insulators grown in-situ in the same chamber. Figure 4a and b show the results measured in devices with SiO₂ and SiN/SiO₂ insulators, respectively. Compared to Fig. 3a, more Coulomb diamonds are overlapped and more uniform opening of the gap around the zero bias condition is observed. More quantum dots are formed and coupled in series. The difference between Fig. 4a and b might be caused by variations in oxidation and absorption of molecules outside the chamber. The result in Fig. 4 is consistent with the expectation that the higher disorder density forms more quantum dots in these devices. These support that the origin of the formation of the quantum dots is the disordered potentials around the FET channels.

In conclusion, we measure electron transport in GaN/AlGaIn FETs at cryogenic temperature. Quantum dots are formed in the conduction channel near the depletion of the 2DEG. Multiple quantum dots are formed by the disordered potential in the FET. We also measured insulator dependence of the quantum dot formation. These results can be utilized for the development of quantum dot devices like semiconductor quantum bits and nano-probes³²⁻³⁴ utilizing GaN/AlGaIn and evaluation of the disordered potential in GaN/AlGaIn FET channels.

Received: 4 April 2020; Accepted: 25 August 2020

Published online: 22 September 2020

References

1. Akasaki, I. & Amano, H. Widegap column-III nitride semiconductors for UV/blue light emitting devices. *J. Electrochem. Soc.* **141**, 2266–2271 (1994).
2. Nakamura, S. & Fasol, G. *The Blue Laser Diode* (Springer, Berlin, 1997).
3. Akasaki, I. Fascinating journeys into blue light (nobel lecture). *Ann. Phys.* **527**, 311–326 (2015).
4. Mishra, U. K., Parikh, P. & Wu, Y. F. AlGaIn/GaN HEMTs—An overview of device operation and applications. *Proc. IEEE* **90**, 1022–1031 (2002).
5. Ikeda, N. *et al.* GaN power transistors on Si substrates for switching applications. *Proc. IEEE* **98**, 1151–1161 (2010).
6. Baliga, B. J. Gallium nitride devices for power electronic applications. *Semicond. Sci. Technol.* **28**, 074011 (2013).
7. Ambacher, O. *et al.* Two-dimensional electron gases induced by spontaneous and piezoelectric polarization charges in N- And Ga-face AlGaIn/GaN heterostructures. *J. Appl. Phys.* **85**, 3222–3233 (1999).
8. Manfra, M. J. *et al.* Electron mobility exceeding $160,000 \text{ cm}^2/\text{Vs}$ in AlGaIn/GaN heterostructures grown by molecular-beam epitaxy. *Appl. Phys. Lett.* **85**, 5394–5396 (2004).

9. Thillozen, N. *et al.* Weak antilocalization in gate-controlled Al_xGa_{1-x}N GaN two-dimensional electron gases. *Phys. Rev. B* **73**, 241311 (2006).
10. Schmult, S. *et al.* Large Bychkov-Rashba spin-orbit coupling in high-mobility GaN Al_xGa_{1-x}N heterostructures. *Phys. Rev. B* **74**, 033302 (2006).
11. Kurdak, C., Biyikli, N., Ozgur, U., Morkoc, H. & Litvinov, V. I. Weak antilocalization and zero-field electron spin splitting in Al_xGa_{1-x}N AlN GaN heterostructures with a polarization-induced two-dimensional electron gas. *Phys. Rev. B* **74**, 113308 (2006).
12. Shchepetilnikov, A. V. *et al.* Electron spin resonance in a 2D system at a GaN/AlGa_xN heterojunction. *Appl. Phys. Lett.* **113**, 052102 (2018).
13. Chou, H. T. *et al.* High-quality quantum point contacts in GaN/AlGa_xN heterostructures. *Appl. Phys. Lett.* **86**, 073108 (2005).
14. Chou, H. T. *et al.* Single-electron transistors in GaN/AlGa_xN heterostructures. *Appl. Phys. Lett.* **89**, 033104 (2006).
15. Ristić, J. *et al.* Columnar AlGa_xN/GaN nanocavities with AlN/GaN Bragg reflectors grown by molecular beam epitaxy on Si(111). *Phys. Rev. Lett.* **94**, 146102 (2005).
16. Songmuang, R. *et al.* Quantum transport in GaN/AlN double-barrier heterostructure nanowires. *Nano Lett.* **10**, 3545–3550 (2010).
17. Nakaoka, T., Kako, S., Arakawa, Y. & Tarucha, S. Coulomb blockade in a self-assembled GaN quantum dot. *Appl. Phys. Lett.* **90**, 162109 (2007).
18. Sellier, H. *et al.* Transport spectroscopy of a single dopant in a gated silicon nanowire. *Phys. Rev. Lett.* **97**, 206805 (2006).
19. Ono, Y. *et al.* Conductance modulation by individual acceptors in Si nanoscale field-effect transistors. *Appl. Phys. Lett.* **90**, 102106 (2007).
20. Tabe, M. *et al.* Single-electron transport through single dopants in a dopant-rich environment. *Phys. Rev. Lett.* **105**, 016803 (2010).
21. Tan, K. Y. *et al.* Transport Spectroscopy of single phosphorus donors in a silicon nanoscale transistor. *Nano Lett.* **10**, 11–15 (2010).
22. Loss, D., DiVincenzo, D. P. & DiVincenzo, P. Quantum computation with quantum dots. *Phys. Rev. A* **57**, 120–126 (1997).
23. Koppens, F. H. L. *et al.* Driven coherent oscillations of a single electron spin in a quantum dot. *Nature* **442**, 766–771 (2006).
24. Yoneda, J. *et al.* Fast electrical control of single electron spins in Quantum dots with vanishing influence from nuclear spins. *Phys. Rev. Lett.* **113**, 267601 (2014).
25. Veldhorst, M. *et al.* A two-qubit logic gate in silicon. *Nature* **526**, 410–414 (2015).
26. Yoneda, J. *et al.* A quantum-dot spin qubit with coherence limited by charge noise and fidelity higher than 99.9%. *Nat. Nanotechnol.* **13**, 102–106 (2018).
27. Nielsen, M. A. & Chuang, I. L. *Quantum Computation and Quantum Information* 7 (Cambridge University Press, Cambridge, 2000).
28. Ladd, T. D. *et al.* Quantum computers. *Nature* **464**, 45–53 (2010).
29. Ono, K., Mori, T. & Moriyama, S. High-temperature operation of a silicon qubit. *Sci. Rep.* **9**, 469 (2019).
30. Ono, K., Tanamoto, T. & Ohguro, T. Pseudosymmetric bias and correct estimation of Coulomb/confinement energy for unintentional quantum dot in channel of metal-oxide-semiconductor field-effect transistor. *Appl. Phys. Lett.* **103**, 183107 (2013).
31. Nuryadi, R., Ikeda, H., Ishikawa, Y. & Tabe, M. Ambipolar Coulomb blockade characteristics in a two-dimensional Si multidot device. *IEEE Trans. Nanotechnol.* **2**, 231–235 (2003).
32. Altimiras, C. *et al.* Tuning energy relaxation along quantum hall channels. *Phys. Rev. Lett.* **105**, 226804 (2010).
33. Otsuka, T. *et al.* Higher-order spin and charge dynamics in a quantum dot-lead hybrid system. *Sci. Rep.* **7**, 12201 (2017).
34. Otsuka, T. *et al.* Difference in charge and spin dynamics in a quantum dot-lead coupled system. *Phys. Rev. B* **99**, 085402 (2019).

Acknowledgements

We thank Takeshi Kumasaka for fruitful discussions and technical supports. Part of this work is supported by ROHM Collaboration Project, PRESTO (JPMJPR16N3), JST, MEXT Leading Initiative for Excellent Young Researchers, Futaba Electronics Memorial Foundation Research Grant, The Mikiya Science and Technology Foundation Research Grant, Harmonic Ito Foundation Research Grant, Takahashi Industrial and Economic Research Foundation Research Grant, The Murata Science Foundation Research Grant, Samco Foundation Research Grant, Casio Science Promotion Foundation Research Grant and The Thermal & Electric Energy Technology Foundation Research Grant.

Author contributions

T. O. and K. N. planned the project; N. I., T. T., and K. N. performed device fabrication; T. O., T. A., T. K., N. I., T. T., and K. N. conducted experiments and data analysis; all authors discussed the results; T. O., T. A., T. K., T. T., and K. N. wrote the manuscript.

Competing interests

The authors declare no competing interests.

Additional information

Supplementary information is available for this paper at <https://doi.org/10.1038/s41598-020-72269-z>.

Correspondence and requests for materials should be addressed to T.O.

Reprints and permissions information is available at www.nature.com/reprints.

Publisher's note Springer Nature remains neutral with regard to jurisdictional claims in published maps and institutional affiliations.



Open Access This article is licensed under a Creative Commons Attribution 4.0 International License, which permits use, sharing, adaptation, distribution and reproduction in any medium or format, as long as you give appropriate credit to the original author(s) and the source, provide a link to the Creative Commons licence, and indicate if changes were made. The images or other third party material in this article are included in the article's Creative Commons licence, unless indicated otherwise in a credit line to the material. If material is not included in the article's Creative Commons licence and your intended use is not permitted by statutory regulation or exceeds the permitted use, you will need to obtain permission directly from the copyright holder. To view a copy of this licence, visit <http://creativecommons.org/licenses/by/4.0/>.

© The Author(s) 2020